IJST (2011) A1: 13-28
Iranian Journal of Science & Technology

http://www.shirazu.ac.ir/en

The application of ASTER imageries and mathematical evaluation method in detecting cyanobacteria in biological soil crust, Chadormalu area, central Iran

A. Moghtaderi[1]*, F. Moore[2], S. M. Taghavi[3] and R. Rezaei[3]

[1]*Department of Geology, College of Sciences, Payam Noor University, Ewaz, Fars province, Iran*
Email: a_moghtaderi@pnu.ac.ir or moghtaderiarsia@gmail.com
[2]*Department of Earth Sciences, College of Sciences, Shiraz University, Shiraz 71454, Iran*
[3]*Department of Plant Protection, College of Agriculture, Shiraz University, Shiraz, Iran*

Abstract

Soil surfaces in arid and semi-arid lands often lack photoautotrophic life but are covered by communities of soil surface covering organisms able to tolerate dehydration, and thus adapted to aridity. One important objective of multi-spectral remote sensing instruments is the detection of the optical characteristics of the Earth's surface using high spectral resolution bands. In this study ASTER imagery and reflected radiation in VNIR bands were used to investigate biological Soil Crusts (BSCs) in the field. By applying IARR (Internal Average Relative Reflectance), FCC (False Color Composite), MNF (Minimum Noise Fraction Transform), and MEM (Mathematical Evaluation Method) techniques, BSCs are successfully detected in the Chadormalu desert area of central Iran. This study clearly shows the capability of ASTER data (VNIR bands) to detect BSC or cyanobacteria soil crusts. The proposed MEM method, despite being approximative is suitable for detecting microorganisms in inaccessible areas such as other planet surfaces or remote areas on earth.

Keywords: ASTER; cyanobacteria; MEM; remote sensing; biological soil crust

1. Introduction

Soil surfaces in arid and semi-arid lands often lack photoautotrophic life but are covered by a community of soil surface organisms that are adapted to aridity and thus able to tolerate dehydration. These communities are known as Biological Soil Crust (BSC) or microphytic soil crust and comprise a complex assemblage of bacteria, cyanobacteria, green algae, microfungi, lichens and mosses [1-3].

This phenomenon has been widely reported from the Middle East [e.g. 4], the African Sahel and Sahara [3], North and South America [5], Central Asia and Australia [3, 6], Northern Victoria Land, McMurdo Dry Valleys and Ice Shelf, Antarctica [e. g. 7] and India [8].

Cyanobacteria and algae are major components of many BSCs [3, 9]. Danin *et al.* [10], Danin [11] and those in the Negev Desert, Israel, consist mostly of cyanobacteria with *Microcoleous vaginatus*; the dominant species accompanied by another cynobacteria genus (e.g. *Scytonema, Schizothrix, Calothrix, Chroococcidiopsis, Nostoc and Phorimidium*) [12]. Similarly, BSCs are present in 4% of the Sonoran Desert [13-15] and comprise up to 70% of the living cover in arid and semiarid areas of the Colorado Plateau Biogeographical Province. Of these organisms, the cyanobacterium *Microcoleous Vaginatus* is estimated to contribute 95% of the soil biomass in shrub and grass interspaces at sites in both the Colorado Plateau and the Great Basin Biogeographical Provinces.

Cyanobacteria structure is similar to that of bacteria (i.e. prokaryote) but their photosynthetic mechanism resembles that of green algae [4, 16, 17]. Cyanobacteria have not only the common chlorophyll *a*, but also phycobilin pigments and many are able to fix atmospheric nitrogen which is needed for proteins. These features, and the lack of complex parts, make it possible for BSCs to occupy an ecological niche in the extreme desert extreme environment.

The cyanobacteria crust, being never more than a few millimeters thick, constitutes a relatively small portion of the soil profile, but since it occupies the uppermost part of the profile, it plays an important role in the desert ecosystem. Danin [11] proposed

*Corresponding author
Received: 11 December 2010 / Accepted: 12 June 2011

that due to the adhesive properties of its filaments, cyanobacteria crust stabilizes the mobile sand dune and prevents water and wind soil erosion. Shields *et al.* [18] showed that it improves soil fertility due to changes in the content of different elements such as amino nitrogen, oxygen, organic carbon and nutrients.

Remote sensing instruments are designed to use the optical characteristics of the Earth's surface to discriminate and map various materials.

To date, little research has been done to spectrally examine biological soil crusts or map them using remote sensing [19]. Karnieli *et al.* [4] have shown that spectral reflectance values can be measured during wet seasons and O' Neill [6], Karnieli and Sarafis [20], Tromp and Steenis [21] and Zombre *et al.* [22], presented spectral curves of cyanobacteria crust. However, none of these authors analyzed, systematically, the spectral features of the cyanobacteria crust through the atmospheric windows available to spectral remote sensing instruments ('i.e. Visible (VIS), Near Infrared (NIR), and Shortwave Infrared (SWIR)) under different moisture conditions.

The ASTER sensor was installed as payload onto an Earth Observing System (EOS) Terra platform and launched on December 18, 1999. It acquires multi-spectral images in14 channels variously spaced through the Shortwave Infrared (SWIR), Visible and Near Infrared (VNIR) and Thermal Infrared (TIR) (Table 1). The VNIR atmospheric window is useful in studying vegetation [23, 24] or, in other words, is an important source of information for studying chlorophyll *a* [25]. This sensor is also a developed multi-spectral sensor which can classify minerals using data from the SWIR region and identify rocks using data from the thermal infrared region [26, 27, 28]. Although ASTER collects data in 9 channels of the VIS, NIR and SWIR, it remains a low resolution instrument and hence is only marginally effective in discriminating the full scope of spectral variety present in a case study. However, for general classification purpose, the new space-born imagers (e.g. ASTER and ALI) present a substantial improvement in spectral mapping capability over older satellite platforms (e.g. Landsat-7ETM) [24]. ALI gives increased spectral resolution in the VNIR compared to Landsat-7ETM. ASTER is cheap, easily available and has the capacity for targeting exploration and land cover studies. [29]. It has an increased spectral resolution in the SWIR compared to Landsat TM and ALI [28, 30]. In other words, ASTER has more bands and better spatial and spectral resolution than Landsat-7ETM and, is cheaper and more available than ALI. Fig. 1 compares the characteristics of ASTER, ALI and Landsat-7ETM.

The BSCs have been detected in the Negev desert, Israel, by a low spectral resolution sensor (i.e. Landsat TM) [31]. Carranza and Hale [32] suggested that, Landsat TM bands 5 and 7 are potentially useful in detecting clay zones in arid areas. However, similarities in shape and relative intensities of the reflection curves of vegetation and clay minerals in the spectral regions covered by Landsat TM bands 5 and 7 make their discrimination difficult (Fig. 1).

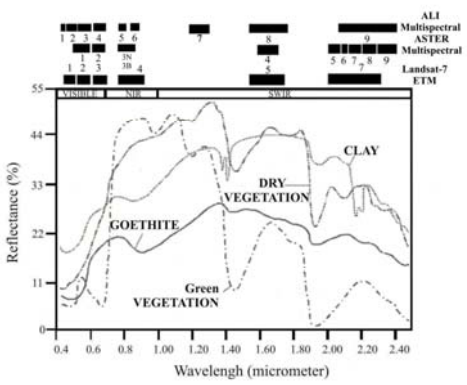

Fig 1. Generalized reflectance spectra of vegetation, clay and iron oxides (Modified from Carranza and Hale, [32]). Note the overlap between clay and vegetation spectral reflectances.

If biological soil crusts (especially cyanobacteria species) extend a wide carpet and are present in sufficient quantities (manifested by chlorophyll *a*) at the surface, from which solar radiation can be reflected to the sensor, then spectroradiometers including ASTER offer the prospect of an additional source of data available to the biologist and environmental geologist [20, 22, 25, 33].

Detecting and mapping a variety of surface features using image data can be obtained by a number of different techniques (e.g. Minimum Noise Fraction (MNF) transform, matched filtering, Principal Component Analysis (PCA) , spectral linear mixture, Biological soil Index, Neural Network) [e.g. 25, 30, 34, 35] but, there has been little work done on soil crusts. Moghtaderi *et al.* [30, 34], using MNF transform and Mathematical Evaluation Method (MEM) techniques on ASTER images showed that the capability and accuracy of the MEM method is better than 2×2 correlated filter technique. This study (MEM and ground control) clearly showed the capability of ASTER data in the detection of alteration minerals in the Chadormalu iron ore deposit, central Iran. The output of applying MEM is a grayscale image, in which the Digital Number (DN) values match the percentage of the alteration mineral present. Kishino *et al.* [25] implemented the neural network (NN) method in

the analysis of ASTER data (VNIR bands) of Tokyo Bay, as a case study in the coastal waters in order to demonstrate the usefulness of remote sensing with high spatial resolution. Their results showed that the indicated concentration of chlorophyll *a* was reasonably accurate. Of course, it is necessary to improve the optical model for simulated data sets as well. Svab *et al.* [35] suggested that PCA, spectral linear modeling and multivariate regression analysis may be used to provide estimates of chlorophyll *a* ((chl *a*)) concentration. None of these methods [25, 35] can record BSCs (e.g. cyanobacteria) with sufficient reliability.

This research is important to discriminate and map such crusts with a low cost readily available data source for desert ecosystem protection and may be useful (MEM method) in astrobiological studies, especially in Mars biological explorations.

In this study an attempt is made to detect cyanobacteria crusts within Chadormalu desert (North of Chadormalu iron deposit). The main purpose is to discriminate and compare the spatial extent of BSC and barren areas.

Table 1. Performance parameters for the ASTER radiometer [30]

ASTER baseline performance requirements						
System	Band number	Spectral Range (μM)	Radiometric resolution	Absolute Accuracy (σ)	Spatial resolution	Signal Quantization levels
VNIR	1	0.52-0.60	NEΔρ≤0.5%	≤ ± 4 %	15 m	8 bits
	2	0.63-0.69				
	3N	0.78-0.86				
	3B	0.78-0.86				
SWIR	4	1.600-1.700	NEΔρ≤0.5%			
	5	2.145-2.185	NEΔρ≤0.5%			
	6	2.185-2.225	NEΔρ≤0.5%	≤ ± 4 %	30 m	8 bits
	7	2.235-2.285	NEΔρ≤0.5%			
	8	2.295-2.365	NEΔρ≤0.5%			
	9	2.360-2.430	NEΔρ≤0.5%			
TIR	10	8.125-8.475				
	11	8.475-8.825		≤ 3 K (200-240 K)		
	12	8.925-9.275	NEΔT≤0.3K	≤ 2 K (240-270 K)	90 m	12 bits
	13	10.25-10.95	.	≤ 1 K (270-340 K)		
	14	10.95-11.65		≤ 2 K (340-370 K)		
Stereo base-to-height ratio	0.6 (along-track)					
Swath width	60 km					
Total coverage in Cross-track direction By pointing	232 km					
Mission life	5 years					
MTF at Nyquist frequency	0.25 (cross-track)					
	0.20 (along-track)					
Band-to-band registration	Intra-telescope:0.2 pixels					
	Intra-telescope:0.3 pixels					
	of coarser band					
Peak data rate	89.2 Mbps					
Mass	406 kg					
Peak power	726 W					
Band number 3N refers to the nadir pointing view, whereas 3B designates the backward pointing view (modified from Rowan and Mars, 2003).						

2. Material and methods

2.1. Meteorological background

The Chadormalu area (including the northern desert) is located in the Bafq metallogenic province in central Iran, about 115 km southeast of Yazd city (55° 15′- 55° 45′E, 32° 15′-32° 25′N) (Fig. 2a, b). The extreme aridity of the Chadormalu desert is due to the Zagros and Alborz mountain ranges to the west and north respectively which prohibit wet (or rainy) weather from reaching this area. Also, the salt deserts (kavir) of Bafq and Saqand occupy the west and north of the Bafq region. The average annual rainfall is 55.7 mm and it only rains in the winter and early spring (January-April). Average minimum daily temperatures are -9.6°C in January and 25°C in May. The average maximum daily temperature is 18°C and 45°C in January and July, respectively.

2.2. Spectral characteristics of cyanobacteria

The spectral reflectance curves (SRC) of surface materials may be used directly to infer natural surface features like the biological soil crust in this research [24, 26, 30, 34]. Laboratory reflectance spectra are accessible over the internet from the USGS (United States Geological Survey) (http://speclab.cr.usgs.gov/spectral.lib04/spectral-lib.desc+plots.html) digital spectral library. These sites provide data on minerals, rocks, vegetation and soils, but there are no data on microphytic (e.g. cyanobacteria) crusts. For this study the most appropriate spectral curve selection criterion is the spectra of dry cyanobacteria crust proposed by Karnieli and Sarafis [20] (Fig. 3a), because it is measured from *Microcoleous Vaginatus* and *Nostoc* which, with *Schizothrix, Calothrix, Chroococcidiopsis and Phorimidium* constitutes the most common cyanobacteria (genus) found in the deserts of the world [10, 11, 36, 37]. In Fig. 3b-f, spectral reflectance curves of soil minerals with grain sizes between 150-500 and ≤ 10 µm are displayed. Although these curves may overlap with spectra of wet cyanobacteria crust, examining the spectral reflectance curves of hematite and goethite indicate that no such overlaps occur in this study.

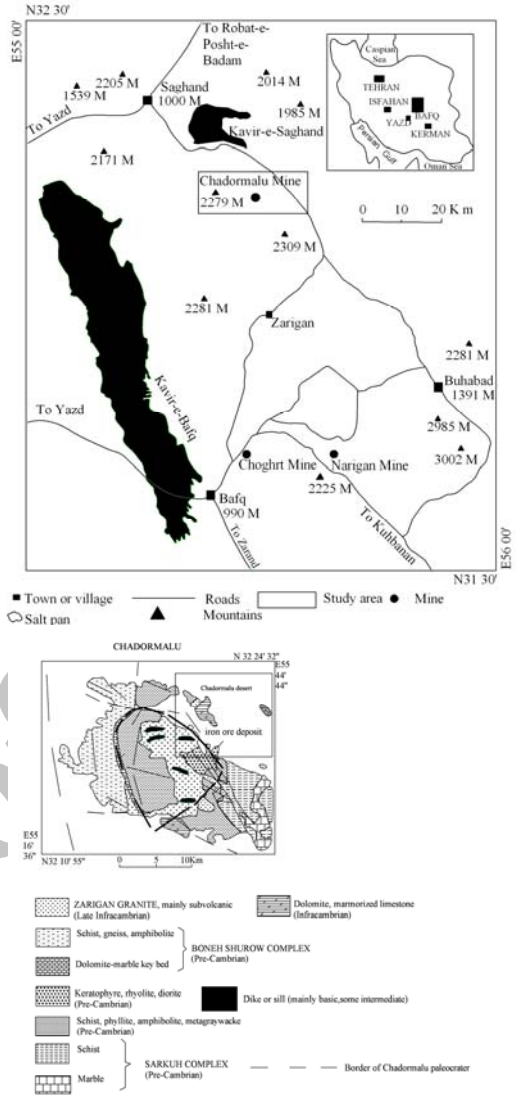

Fig. 2 (a). Location of Chadormalu desert area in central Iran [30], (b) Geological map of Chadormalu desert and Chadormalu iron oxide deposit (bordered area) (Modified from Moghtaderi et al., [30])

The wavelength positions, reflectance, depth and number of spectral absorption features define the diagnostic features of any material (including microphyts) and hence provide the basis for mapping $BSC_{(s)}$ [38]. Sharp fluctuations in the reflectance spectral curves for cyanobacteria were used to determine the best ASTER bands (3, 2, 1 bands) for the detection of cyanobacteria (‘i.e. *M. vaginatus* and *Nostoc*) (Fig. 3a Table 2).

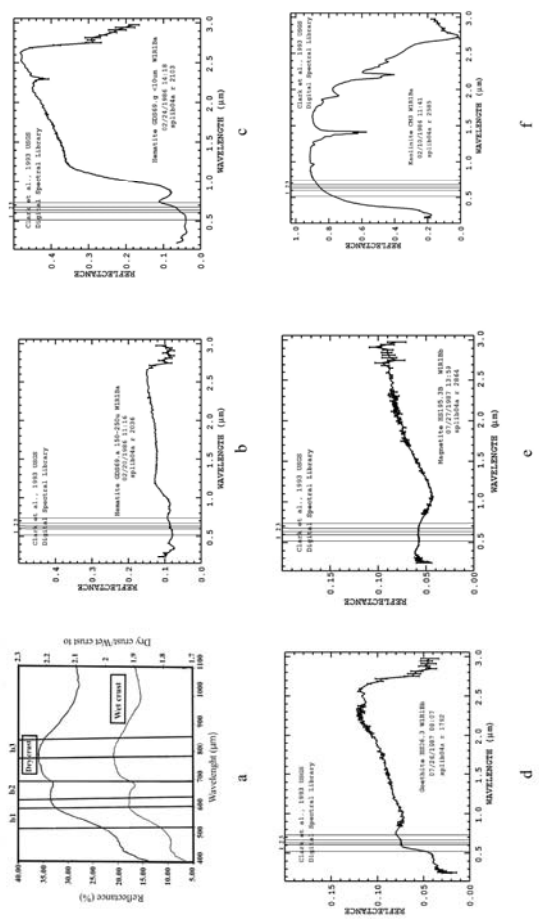

Fig. 3(a). Spectral reflectance curve of Cyanobacteria in dry and wet conditions (Modified from Karnieli and Sarafis, [20]) (nm = Nanometer) compared with clay and Iron minerals (Fig. 3b-f) including the Hematite, goethite, magnetite, and kaolinite respectively, in each figure, there is no overlap between Fig. 3a and spectral reflectance curves of clay and Iron minerals, especially in dry condition.

Table 2. Reflectance values of the dry and wet conditions of cyanobacteria extracted from Karnieli and Sarafis [20]

Cyanobacteria	VNIR bands		
	1	2	3
Dry conditions	0.31	0.33	0.36
Wet conditions	0.18	0.17	0.21

2.3. ASTER image processing and methodology

ASTER Image processing was carried out according to the following steps:

1) Initially, bands 1, 2, 3 were selected from the 14 bands available in ASTER imagery, as these bands contain the most discriminatory information for the spectral curves of cyanobacteria [20].

2) ASTER level-1B data are radiance at the sensor, and not reflectance. In order to directly compare multi-spectral image spectra with reference spectra, the encoded radiance value in the image must be converted to reflectance [12]. The Internal Average Relative Reflectance (IARR) method in ENVI software was applied on the ASTER radiance data to obtain relative reflectance images and then a false color composite (FCC) image was created from the reflectance data. The IARR is pseudoreflectance, and although this is not true reflectance, it has been shown to be directly proportional to true reflectance, and therefore values obtained from such data should be proportional to real reflectance. According to Kruse et al. [39], Kruse [40] and Van der Meer [41] the IARR calibration method normalizes images to a scene average spectrum or normalizes the data by scaling the sum of the input pixel values in each spectral band for each pixel to a constant value. This shifts all spectral radiances to the same relative brightness. This is particularly effective for reducing imaging spectrometer data to relative reflectance in an area where no ground measurements exist and little is known about the scene. This method requires no knowledge of the surface materials because it uses an average effective spectral radiance calculated directly from the input data. Apparent reflectance is calculated for each pixel of the image by dividing the scene average spectrum into the spectrum for each pixel. In other words, the effective spectral radiance of each pixel in the image is divided by the average effective spectral radiance. The average spectral radiance is also thought to contain solar irradiance. The resulting spectral values represent reflectance relative to the average spectrum. The procedure removes the majority of the atmospheric effects, except in cases when the area has wide variations in elevation, or where atmospheric conditions are not uniform across the image. It works best for arid areas with no vegetation. Thus, the final outputs (MEM's digital numbers) in this research are not real reflectance values, but are proportional to them.

3) FCC was composed using bands 3, 2, 1(RGB).

4) A forward minimum noise fraction (FMNF) transform was carried out on the FCC to identify the noise within the image [26, 28, 42]. The FMNF procedure is similar to PCA. The main difference is that the FMNF considers the noise, while PCA observes the data variation. The FMNF performs an ordering component method according to maximum variance. The dimensionality of image data can be reduced for processing algorithms by working in FMNF space and ignoring noisy bands, and using only bands containing useful information. The FMNF transformation is used to determine the

dimensionality of the image data, separate noise in the data, and to reduce the computational requirements for subsequent processing [43].

5) After applying a linear image enhancement (2%) to the resultant FMNF images of the fourth step, an inverse MNF transform (Fig. 4a) is applied to return the data from FMNF space to spectral space in a cleaner form.

Fig. 4(a)

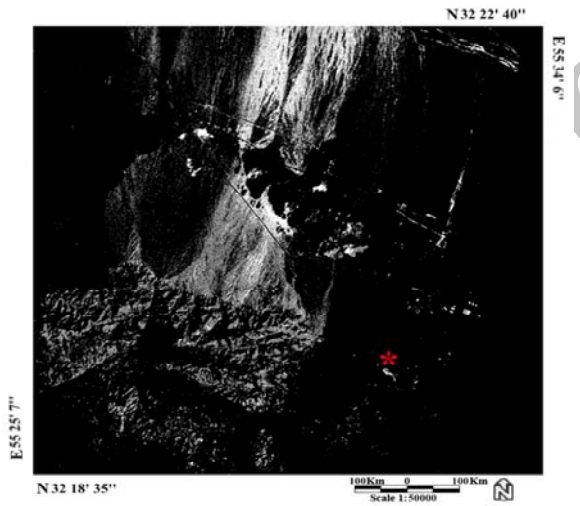

Fig. 4(b)

So, we are applying an inverse or reverse MNF but not taking out any of the noise bands. This way, the contrast/stretch of the MNF bands is adjusted to eliminate extreme values, essentially clipping the FMNF data.

6) The MEM method is applied to the inverse MNF data. This data was used as input for the MEM process.

The degree of the proximity of the input DN (Digital Number) values to the cyanobacteria reflectance values (Table 2) was calculated using the following formula proposed by Moghtaderi et al. [30, 34]:

$$M = \begin{bmatrix} M_{i,j,1} \\ M_{i,j,2} \\ M_{i,j,3} \end{bmatrix}_{m \times n \times 3}$$

$$1 \le i \le m \quad , \quad 1 \le j \le n$$

$$N_{i,j} = \frac{1}{3} \sum_{b=1}^{3} \left(\frac{M_{i,j,b}}{255} - R_b \right)^2$$

$$N = \left\lfloor N_{i,j} \right\rfloor_{m \times n}$$

$$1 \le i \le m \quad , \quad 1 \le j \le n$$

Where m, n is the number of rows and columns of the input or output image; b=1, 2, 3 is the number of bands of the input FMNF cleaned data; R_b is the reflectance value of the cyanobacteria in band b for VNIR bands; $M_{i,j,b}$ is the pixel DN value of the input FMNF cleaned image in band b which is in [0,255] domain; $N_{i,j}$ is the output calculated DN value of the grayscale image which is in [0.00,1.00] domain; i, j is the number of row and column of a pixel from the input or output image. M is the input FMNF cleaned data; N is the output gray scale image.

The output of applying MEM is a gray scale image, in which the DN values correlate with the percentage of the cyanobacteria (i.e. *M. Vaginatus* and *Nostoc*) present. For example a pixel DN value of 36% (0.36) for a cyanobacteria show a high occurrence of the microorganism living in the region of interest. For a pixel $M_{i,\,j,\,1:3}$ from input image $M_{m \times n \times 3}$, the output gray scale image $N_{m \times n}$ with a DN value of $N_{i,j}$ will be as the above mathematical formula.

The following criteria are used for the interpretation of the $N_{i,\,j}$ amounts:

A pixel DN value $0.00 \le N_{i,j} \le 0.11 \Rightarrow$ Very low (trace) amount of a cyanobacteria and is shown with black color; A pixel DN value $0.11 \le N_{i,j} \le 0.30 \Rightarrow$ Low (minor) amount of a cyanobacteria and is shown with gray color; A pixel DN value $0.30 \le N_{i,j} \le 0.400 \Rightarrow$ High (major) amount of a cyanobacteria and is shown with white color.

The cyanobacteria component which is present in the greatest amount is shown with brighter pixels; these pixels indicate a greater amount of a cyanobacterium.

The human eye responds more readily to rainbow color than gray scale, so the MEM is presented as a pseudocoloured image in rainbow colors (Fig. 4c). In this transform, subsetting data was done by using

the MEM file. High pass kernel and low pass sizes are 36 and 11 are derived from DN contents of major and trace amounts of cyanobacteria, respectively. The saturation value is 0.5 and dark and pale pink colors correspond to major amounts (DN=0.3-0.36) of the microorganisms, while, green, yellow, cyan, and blue colors represent minor amounts (DN=0.11-0.30), and trace amounts (DN=0.00-0.11) are represented in dark red color.

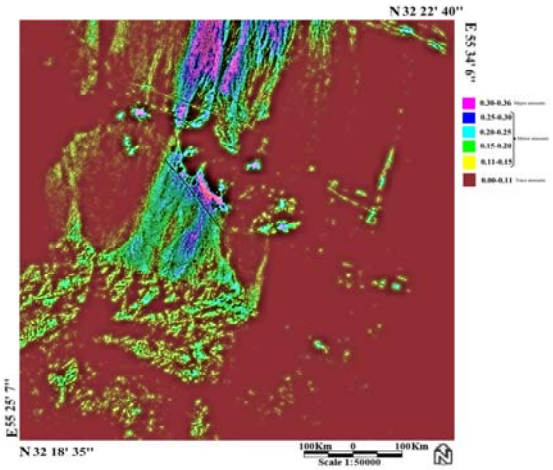

Fig. 4(c)

Fig. 4(a-c). Inverse MNF image (bands 3, 2, 1) of Chadormalu desert and Chadormalu iron deposit. (b) Detected cyanobacteria soil crust (MEM 3 2 1) in Chadormalu desert and iron mine (*area). (c) MEM321 pseudo color display, dark and pale pink colors correspond to major amounts (DN=0.3-0.36) of the microorganisms, while green, yellow, cyan, and blue colors represent minor amounts (DN=0.11-0.30) and trace amounts (DN= 0.00-0.11) are represented in a dark red color

2.4. Ground control

2.4.1. Field study

Field study (ground control) was carried out in late April (18-24 April) in dry conditions, thus dry crust SRC was performed on the ASTER image data. Before performing SRC the metrological data was checked to make sure that there was no rainfall in the days preceding data capture.

As a first step 14 sampling stations were selected by the authors in white, gray and black pixels (Fig. 5). Their coordinates were determined from the georeferenced ASTER data using ENVI 4.7 SP1 (Cursor location/value window) (Fig. 5, Table 3). The data is orthocorrected, which was georeferenced and processed by AGARSS Ltd Company, Australia (to an accuracy of ± 45m~ 3 pixels). The selection of sampling stations was done on areas with a high density of white and gray pixels (major and minor amounts). In other words, the selection of soil sampling stations was carried out in a way that the soil sampling errors would be decreased.

In the field, the location of every sampling station was confirmed by GPS instrument (*etrex, Vista Garmin*) (Table 3) However, the horizontal error of the instrument is about 10m; hence soil sampling is an approximation within a 15m^2 domain (soil samplings were done from thick soil covers).

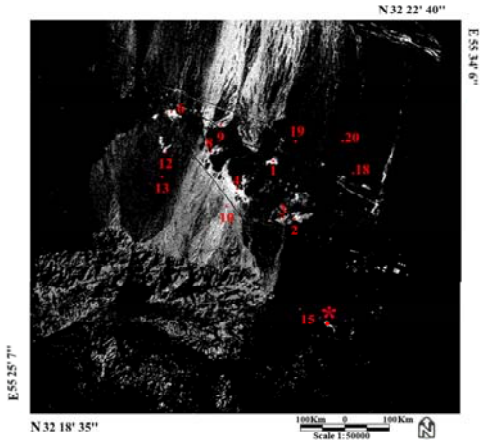

Fig. 5. Soil sampling stations at Chadormalu desert. Each sampling station is shown by a dark red spot.

Table 3. Coordination and culturing results of cyanobacteria soil crust at Chadormalu desert area

Sample code Culturing result	Coordination	Genus and Species
Cyb1 +	N32 21 1.71, E55 30 18.5	*Microcystis*
Cyb2 +	N32 19 56.42, E55 30 30.5	*M. vaginatous*
Cyb3 +	N32 19 57.5, E55 30 16.8	*Chroococcidiopsis*
Cyb4 +	N32 20 36.8, E55 29 28.7	*Nostoc. spp*
Cyb6 +	N32 22 12.1, E55 28 30.1	*Microcystis*
Cyb8 +	N32 21 23.4, E55 29 9.1	*M. vaginatous*
Cyb9 +	N32 21 49.6, E55 29 25.3	*Nostoc. spp*
Cyb10 -	N32 20 22.3, E55 29 13.9	-
Cyb12 +	N32 21 33.7, E55 28 13.0	very small, ND
Cyb13 +	N32 21 5.7, E55 28 8.1	*Nostoc. spp*
Cyb15 +	N32 17 55.1, E55 30 46.1	*Nostoc. spp*
Cyb19 - Cyb20 - Cyb18 -	N32 21 14.63, E55 30 59.2 N32 21 12.02, E55 31 50.6 N32 20 36.07, E55 31 55.6	- - -

ND=Not determined

At each station, soil was picked up (3cm thick) and retained in plastic bags and then transported (in darkness, 25$^{\circ C}$) over a period of days with no apparent loss of viability. Castenholze [44] protocol was followed in this study.

2.4.2. Culturing, isolation and purification

In the laboratory, BG-11 media was used as culture media as described by Hughes *et al.* [45] and modified by Allen [46]. Medium BG-11 has been widely used for isolation and maintenance of many cyanobacteria (about 300 axenic strains), and is a general media culture of cyanobacteria.

Medium BG-11 has low phosphate content, is poorly buffered, and has the following composition (in grams per liter of deionized distilled water): $NaNO_3$, 1.5; K_2HPO_4, 0.04; $MgSO_4.7H_2O$, 0.075; $CaCl_2.2H_2O$, 0.036; Citric acid, 0.006; Ferric ammonium citrate, 0.006; EDTA (disodium magnesium salt), 0.001; Na_2CO_3, 0.02; Trace-metal mix A5, 1ml/lit. Trace-metal mix A5 is included: H_3BO_3, 2.86 g/liter; $MnCl_2.4H_2O$, 1.81 g/liter; $ZnSO_4.7H_2O$, 0.222 g/liter; $Na_2MoO_4.2H_2O$, 0.39 g/liter; $CuSO_4.5H_2O$, 0.079 g/liter; $Co(NO_3)_2.6H_2O$, 0.0494 g/liter (after autoclaving and cooling, pH of medium was 7.1) [47]. Solid media were prepared by mixing equal volumes of separately autoclaved double strength solutions of the mineral salts medium and either purified agar or agarose after cooling to 50°C (autoclave sterilization temperature) to give a final concentration of 0.6% [44, 48]. In other words, we simulate field climatic and seasonal conditions.

After soil solution preparation in deionized distilled water, a two stage serial dilution was performed on the (original) solution. The final soil solutions (final types) were cultured in the solid mediums (BG-11). During isolation and purification, cultures were incubated in a light-dark cycle with a 14-h light period and a 10 dark period for one to two weeks. The temperature of incubation was 20-30°C or room temperature [44, 47, 48, 17].

3. Results

3.1. Image interpretation

MEM (bands 3, 2, 1) show white and gray pixels or high (major) to low (minor) amounts of cyanobacteria (Fig. 4b) in the Chadormalu desert. Elsewhere in the area, white and gray pixels are interpreted to represent thick soil cover (Fig. 11a-c) and black pixels represent thin soil cover (Fig. 11 d, e). At Chadormalu iron mine (Fig. 4b and Fig. 11f) there are no white or gray pixels. According to Belnap [49], just as plants increase or decrease with livestock grazing, many biological soil crust components (e.g. cyanobacteria) are good indicators of *a lack of* physical disturbance, such as by livestock, human foot traffic, motorized vehicles and mining activity (e.g. Fig. 4a and Fig. 11g). Thus, the black pixels in this area are taken to indicate the degree of disturbance in the area caused by mining.

3.2. Microbiology laboratory studies

The cyanophytes in fully propagated colonies were identified in the solid BG-11 culture media after 1 to 2 weeks. The cultures were then examined by a phase-contrast microscope to determine genus and species. They mostly included: *Microcoleous vaginatus* (Fig. 6a-d), *Nostoc.sp* (Fig. 7a-d), *Microcystis.sp* (Fig. 7e), *Ocillatoria.sp* (Fig. 8a), *Chroococcuss.sp* (Fig. 8b) and *Chroococcidiopsis* (Fig. 8c, d). They were found to correspond with the black pixels, especially; sampling stations 1, 2, 4, 6 and 8 (Fig. 5). In the station 6, an artificial pond was found to contain *Ocillatoria.sp, Chroococcuss.sp* and Green float *Microcystis.sp* colonies (Fig. 8e, f). No cyanophytes were found to propagate in the cultures media of black pixels (e.g. stations 18, 19, 20) (Fig. 9c, l, and k). Station 10 is located in gray pixels, however, soil contamination by gasoline, foot traffic and motorized vehicles disturb cyanobacteria soil crust (Fig. 9i and Fig. 11h-i). Fig. 9 a-n illustrates culture media after 2 weeks. Fig. 10 a-d illustrates the natural environments of *Microcoleous vaginatus*, *Nostoc.sp* and *Chroococcidiopsis* at Chadormalu soil desert (e.g. stations 2, 8, 4 and 3).

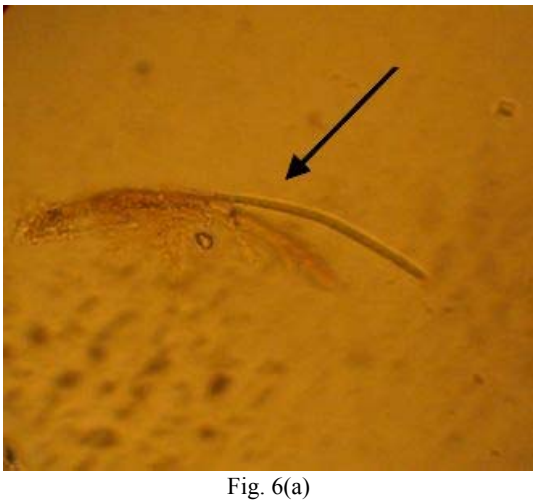

Fig. 6(a)

Fig. 6(b)

Fig. 6(c)

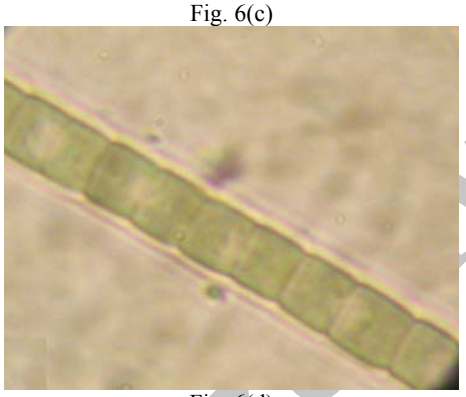

Fig. 6(d)

Fig. 6(a-d). *Microcoleous vaginatus* in 4x, 10x, 40x and 40x magnification, respectively

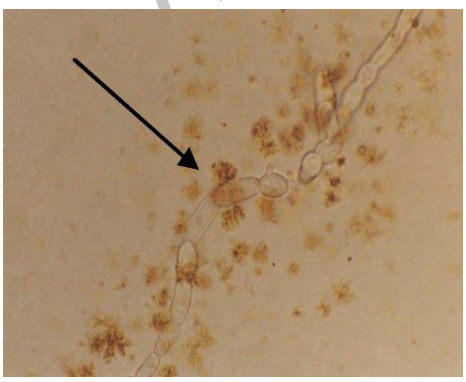

Fig. 7(a)

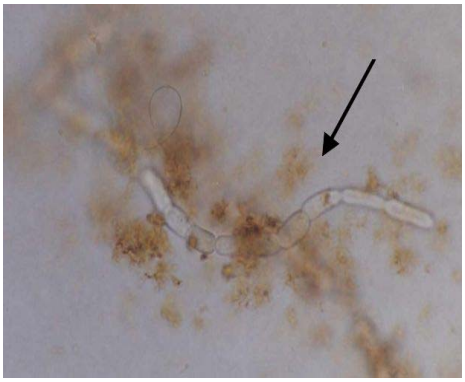

Fig. 7(b)

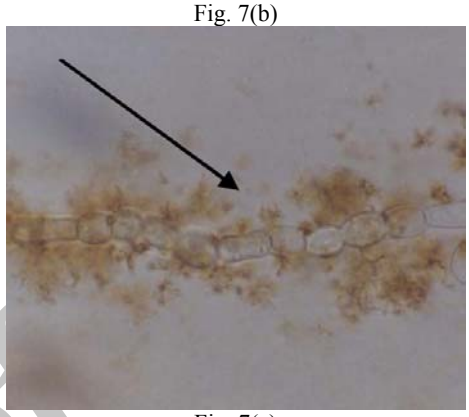

Fig. 7(c)

Fig. 7(d)

Fig. 7(e)

Fig. 7(a-e). a *Nostoc* filamentous with 10x, 40x, 60x magnifications (phase microscope). (d) *Nostoc* filamentous in 40x magnifications (TM). (e) Microcystis colony under TEM (28000x). *TM= Transmitted microscope, TEM=Transmitted Electron Microscope*

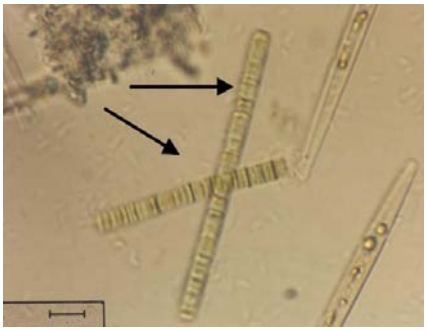

Fig. 8(a)

Fig. 8(b)

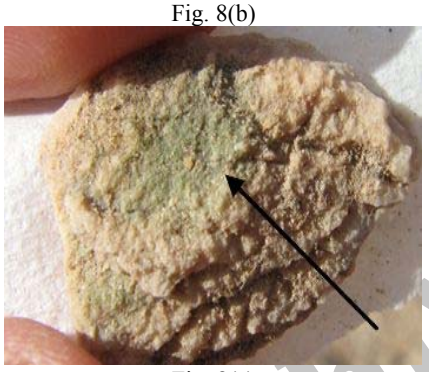

Fig. 8(c)

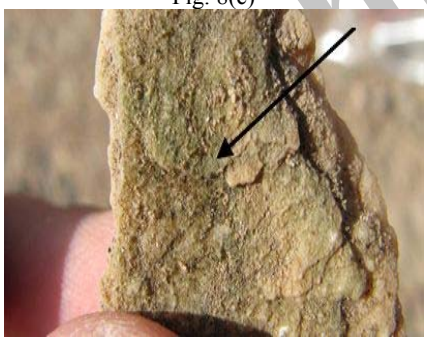

Fig. 8(d)

Fig. 8(e)

Fig. 8(f)

Fig. 8(a-f). *Ocillatoria.spp* filamentous (40x); (a) were prepared by phase microscope. (b) unicellular *Chroococcuss.spp* (40x, phase microscope). (c) and (d) Endolithic cyanobacteria (*Chroococcidiopsis*). (e) and (f) an artificial pond and green float *Microcystis.spp* colonies

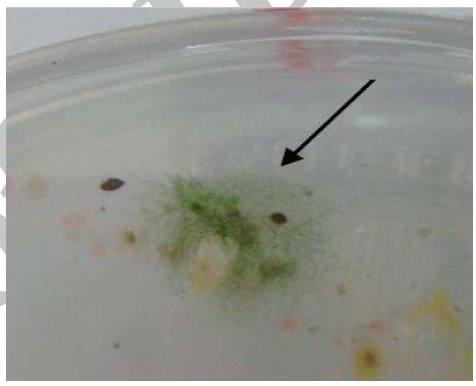

Fig. 9(a)

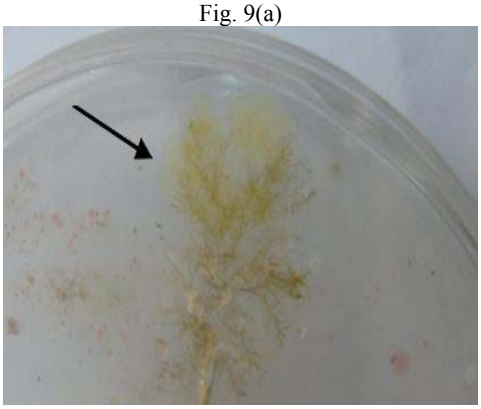

Fig. 9(b)

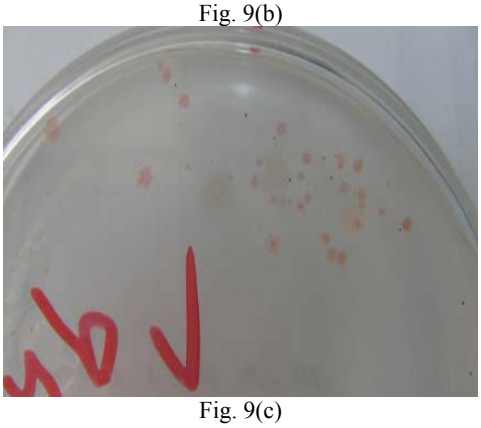

Fig. 9(c)

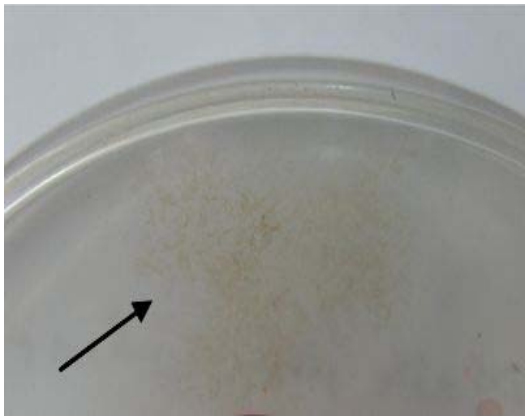

Fig. 9(d)

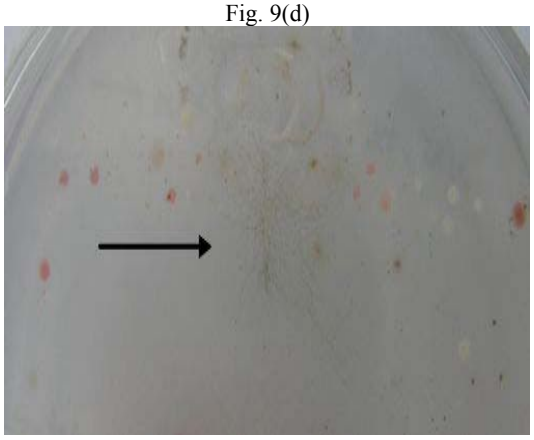

Fig. 9(e)

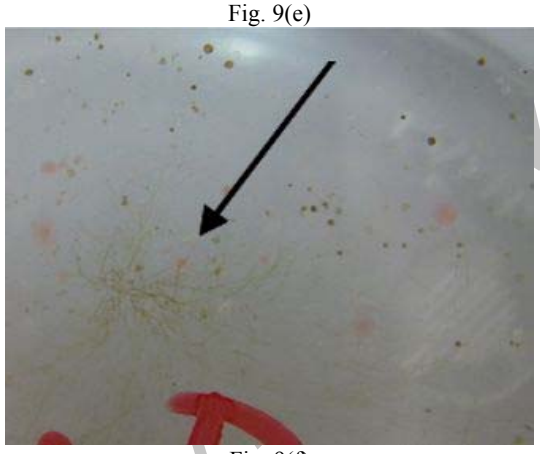

Fig. 9(f)

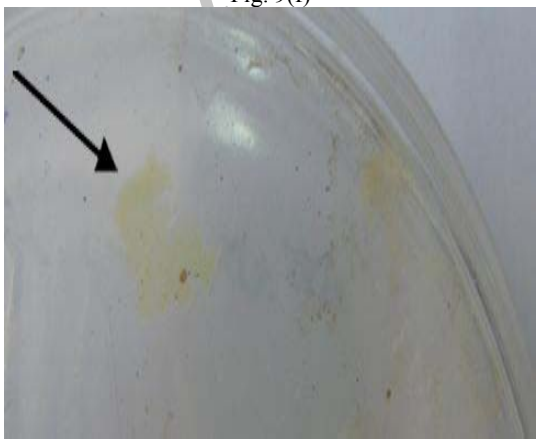

Fig. 9(g)

Fig. 9(h)

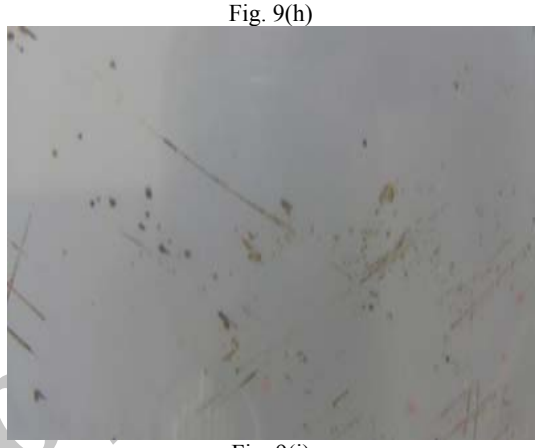

Fig. 9(i)

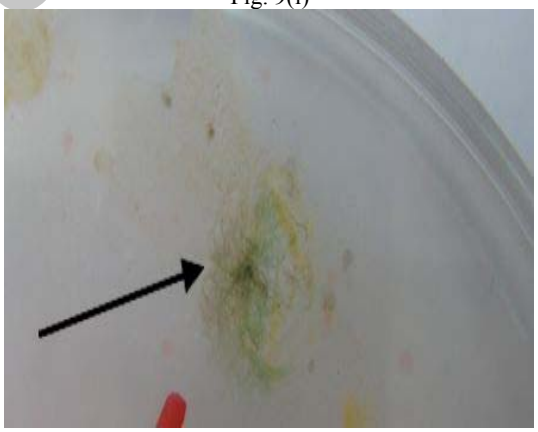

Fig. 9(j)

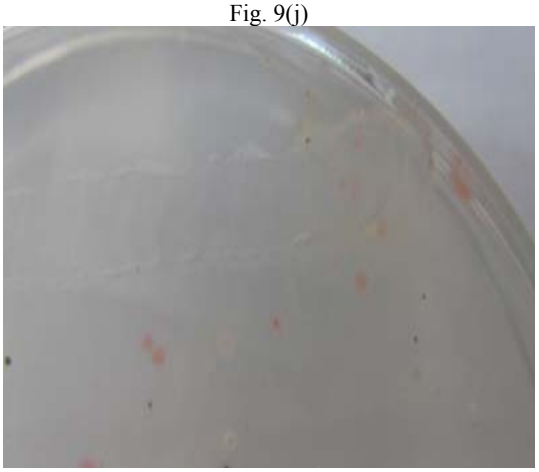

Fig. 9(k)

Fig. 9(l)

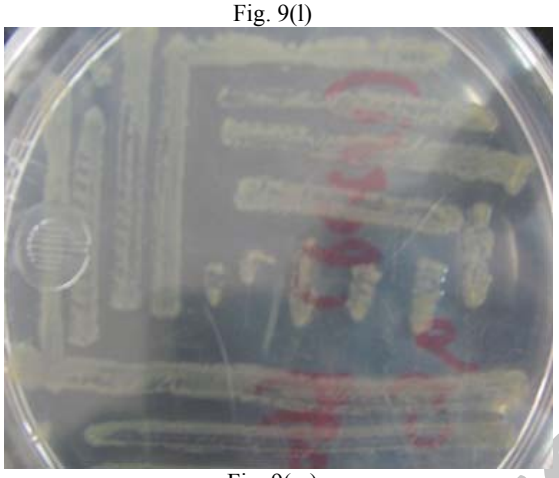

Fig. 9(m)

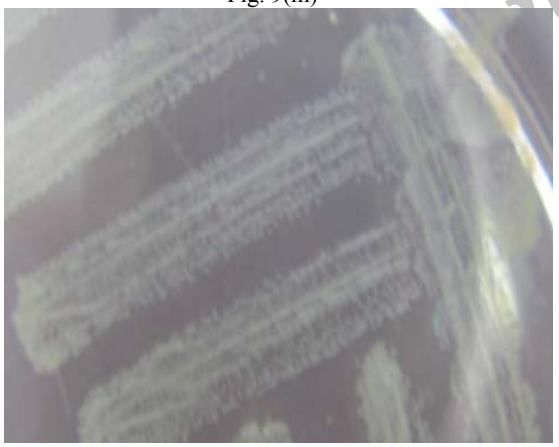

Fig. 9(n)

Fig. 9(a-n). Cyanobacteria growth after 2 weeks (Ref to Fig.4b, Fig. 5 and table. 3). (a) *Microcoleous vaginatus* colony at station-8 (cyb8). (b) *Nostoc.spp* colony at station-4 (cyb4). (c) negative result at station-18 (cyb18). (d-f) *Nostoc.spp* colonies at stations 13 (cyb13), 9 (cyb9) and 15 (Cyb15) respectively. (g) *Microcystis* at station-1 (cyb1). (h) very small cyanobacteria colony. (i) negative result at station-10 (cyb10). (j) *Microcoleous vaginatus* colony at station-2 (cyb2). (k-l) negative results at stations 20(cyb20), 19 (cyb19). (m) and (n) *Microcystis* colony at station-6, artificial pond (Fig. 8f) and soil respectively

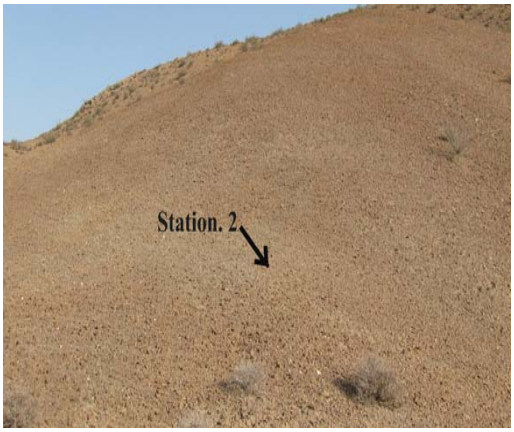

Fig. 10(a)

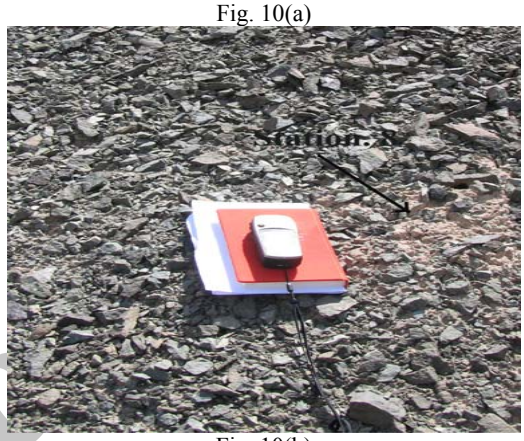

Fig. 10(b)

Fig. 10(c)

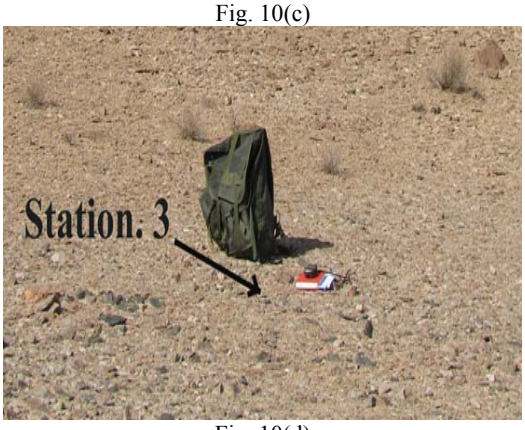

Fig. 10(d)

Fig. 10(a-d). Manifestation of soil at stations 2, 8, 4 and 3

Fig. 11(a)

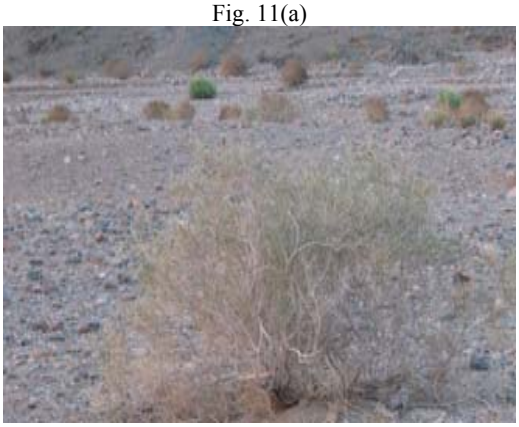

Fig. 11(b)

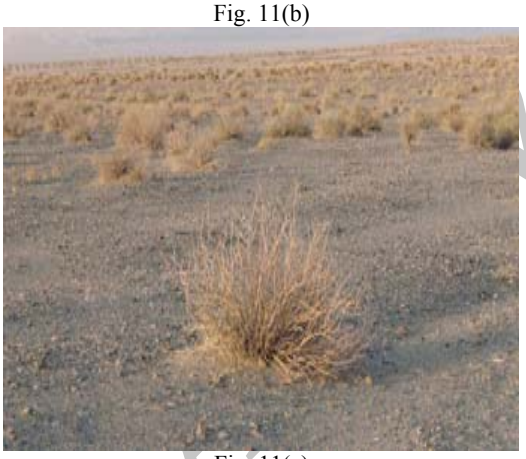

Fig. 11(c)

Fig. 11(d)

Fig. 11(e)

Fig. 11(f)

Fig. 11(g)

Fig. 11(h)

Fig. 11(i)

Fig. 11(a-i). (a, b) Rich soil area in Cyb1 soil sampling station with high vegetation cover (c) Rich soil area in Cyb9 soil sampling station with higher vegetation cover than Cyb1 (d, e) Barren area at Cyb19 soil sampling station (f) mining activity at Chadormalu iron deposit (g) motorized vehicles activity at Chadormalu iron deposit (h) soil contamination by gasoline (i) Foot traffic and motorized vehicles activity at Cyb10 soil sampling station

4. Discussion

The extent of cyanobacterial blooms has been mapped using different satellite sensors [e.g. 50-55]. Gones et al. [50] used one of the first satellite sensors, MERIS (satellite-based digital imagining spectrometers with a less than 1-km spatial resolution and suitable spectral band width) that can be applied to map cyanobacterial distributions in inland waters (i. e. Lake Ijsselmeer, Netherlands). Based on retrieval algorithms to estimate phycocyanin, MERIS data can produce synoptic views of cyanobacterial bloom formation and dispersal. These authors suggested that airborne, spaceborne remote sensings and shipboard observation need to be exploited in concreted programmes of data acquisition, validation and reporting in summer time. The amount of chlorophyll-α is extremely variable spatially [53]. Simis et al. [55] have shown that their reflectance band-ratio algorithm for retrieval of cyanobacterial phycoyanin concentration (PC) decreased gradually with time in Lake Ijsselmeer throughout the period April–September (when cyanobacterial abundance is known to be high). Therefore, these studies did not capture the seasonal variability necessary for a more complete validation procedure [54].

Kutser et al. [51] show that MODIS band 1 response to changes in the concentration of cyanobacteria is nonlinear. Band 1 response is strongest in the case of *Nodularia spumigena*, indicating that quantitative mapping of this species in bloom conditions is easier than in the case of the other species of cyanobacteria investigated. However, these researchers infer that quantitative mapping of cyanobacteria may be impossible by remote sensing sensors due to the opaqueness of the scum and variability in the properties of cyanobacteria within the scum.

According to Kutser [52] quantitative detection of chlorophyll in cyanobacterial blooms by remote sensing has been less successful. This author demonstrates that, it is difficult to collect representative water samples from research vessels using standard methods because ships and water samplers destroy the natural distribution of cyanobacteria in the sampling process. Flow through systems take water samples from the depths at which the concentration of cyanobacteria is not correlated with the amount of phytoplankton that remote sensing instruments detect. Also, the chlorophyll estimation accuracy in cyanobacterial blooms by many satellites is limited because of spatial resolution, as significant changes in chlorophyll concentration occur, even at a smaller spatial scale than 30 m (e.g. ALI, ASTER and Hyperion). In other words, the chlorophyll estimation accuracy in cyanobacterial blooms by remote sensing satellites (e.g. SeaWiFS, MERIS and MODIS) is limited as a result of their coarse spatial resolution and the fine spatial phenomena present in a bloom. The real chlorophyll values in dense cyanobacterial blooms can only be estimated from remote sensing data. This, however, requires detailed knowledge about optical properties of the bloom, knowledge that is currently not available.

In this research, for the first time, a mathematical evaluation method was applied on the ASTER imagery data of a solid environment (Chadormalu desert soil), in dry or extreme conditions. Also, it must be noted that ASTER bands (3, 2, 1 bands) have a higher spatial resolution (15m) than sensors used in the previous work. On the other hand, as mentioned above (Ref. to IARR concept), this method (MEM) is a relative estimation with a full scope view. On the basis of instrumental analysis limitation, especially the lack of a portable spectrometer, the obtained results must be considered approximations at their best. However, the proposed method is a fast technique that takes little time, is comparatively cheap, and is suitable for reconnaissance stages.

5. Conclusion

The above proposed MEM method, despite being approximate is suitable in detecting microorganisms (e.g. cyanobacteria) in inaccessible areas such as other planet surfaces or remote areas on earth, being most useful in extreme dry conditions.

Acknowledgements

The authors wish to thank the Plant Protection and Earth Sciences Departments of Shiraz University. The research council of Pyam Noore University is also thanked for supporting this research. Thanks are also due to Dr. Bob Agar, director of AGARSS Pty. Ltd. Australia, for providing the ASTER imageries.

References

[1] Belnap, J. & Lange, O. L. (2001). *Biological Soil Crust: Structure, function and management*. New York, USA: Springer.

[2] Warren, S. D. (1995). *Ecological role of microphytic soil crusts in arid ecosystems*. In Microbial diversity and ecosystem function, D. Allsopp, D. L. Hawksworth, & R. R. Colwell (Eds.), London, UK: Cab International.

[3] West, N. E. (1990). Structure and function of microphytic soil crusts in wild land ecosystems of arid and semi-arid regions. *Advances in Ecological Research, 20,* 197-223.

[4] Karnieli, A., Kidron, G. J., Glaesser, C. & Ben-Dor, E. (1999). Spectral characteristics of cyanobacteria soil crust in semiarid environment. *Remote Sensing of Environment, 69,* 67-75.

[5] Wierzchos, J., Ascaso, C. & McKay, C. P. (2006). Endolithic cyanobacteria in halite rocks from the hyperarid core of the Atacama Desert. *Astrobiology, 6,* 1-8.

[6] O'Neill, A. L. (1994). Reflectance spectra of microphytic soil crusts in semi-arid Australia. *International Journal of Remote Sensing, 15,* 675-681.

[7] Rios, A., Ascaso, C., Wierzchos, J., Valient, E. F. & Quesada. A. (2004). Microstructural characterization of cyanobacterial mats from the McMurdo Ice Shelf, Antarctica. *Applied and Environmental Microbiology, 70,* 569-580.

[8] Tirkey, J. & Adhikary, S. P. (2005). Cyanobacteria in biological soil crusts of India. *Current Science, 89,* 515-521.

[9] Belnap, J. (1990b). Microbiotic crusts: their role in past and present ecosystems. *Park Science, 10*, 3-4.

[10] Danin, A., Bar-or, Y., Dor, I. & Yisraeli, T. (1989). The role of cyanobacteria in stabilization of sand dunes in southern Israel. *Ecologia Mediterranea, 15,* 55-64.

[11] Danin, A. (1991). Plant adaptation in desert dunes. *Journal of Arid Environment, 21,* 193-212.

[12] Lau, I. C. (2004). Regolith-Landform and mineralogical mapping of the white Dam prospect, eastern Olary domain, South Australia, using integrated remote sensing and spectral techniques, Ph.D. thesis, University of Adelaide, Australia, 369pp.

[13] Anderson, D. C., Harper, K. T. & Rushforth, S. R. (1982b). Recovery of cryptogamic soil crusts from grazing on Utah winter ranges. *Journal of Range Management, 35*, 355-359.

[14] Belnap, J. (1993). Recovery rates of cryptobiotic crusts: inoculants use and assessment methods. *Great Basin National park, 53,* 89-95.

[15] Campbell, S. E., Seeler, J. & Golubic. S. (1989). Desert crust formation and soil stabilization. *Arid Soil Research and Rehabilitation Journal (New title: Arid Land Research and Management), 3,* 217-228.

[16] Konhauser, K. (2006). *Introduction to geomicrobiology*. Singapore, Blackwell publishing.

[17] Waterbury, J. B. (2006). *The cyanobacteria-Isolation, Purification and Identification*. In The prokaryotes, a handbook on biology of bacteria, M. Dworkin, S. Falkow, E. Rosenberg, K. H. Schleifer, *E.* Stackebrandt (Eds.), Germany, Springer.

[18] Shields, L. M., Mitchel, C. & Drouet, F. (1957). Alga and lichen-stabilized surface crusts as soil nitrogen sources. *American Journal of Botany, 44,* 489-498.

[19] Ager, C. M. & Milton, N. M. (1987). Spectral reflectance of Lichens and their effects on the reflectance of rock substrates. *Geophysics*, *52*, 898-906.

[20] Karnieli, A. & Sarafis, V. (1996). Reflectance spectrometry of cyanobacteria within soil crusts - a diagnostic Tool. *International Journal of Remote Sensing, 17,* 1609-1615.

[21] Tromp, M. & Steenis, Z. (1996). Deriving sub-pixel soil characteristics in Northern Burkina Faso with spectral unmixing. *In proceedings of the ISSS International Symposium (Working Group RS and DM) on Monitoring Soils in the Environment with Remote Sensing and GIS, 1995,* Ouagadougou, Burkina Faso, 269-284.

[22] Zombre, P. N., Pallo, F. & Mulders, M. A. (1996). Excursion to the Kaya region, Burkina Faso. *In proceedings of the ISSS International Symposium (Working Group RS and DM) on Monitoring soils in the Environment with Remote Sensing and GIS, 1995, (Eds.),* Ouagadougou, Burkina Faso, 569-592.

[23] Aronof, A. (2005). Remote Sensing for GIS Managers. California, USA: ESRI Press, Redlands.

[24] Lillesand, T. M., Kieffer, R. W. & Chipman, J. W. (2004). *Remote Sensing and Image Interpretation.* USA: Wiley.

[25] Kishino, M., Tanaka, A. & Ishizaka, J. (2005). Retrieval of chlorophyll *a*, suspended solids, and colored dissolved organic matter in Tokyo Bay using ASTER data. *Remote Sensing of Environment, 99,* 66-74.

[26] Ferrier, G., White, K., Griffiths, G., Bryant, R. & Stefouli, M. (2002). The mapping of hydrothermal alteration zones on the island of Lesvos, Greece, using an integrated remote sensing data set. *International Journal of Remote Sensing, 23,* 341-356.

[27] Rowan, L. C., Kingston, M. J. & Crowley, J. K. (1986). Spectral reflectance of carbonatite and related alkalic igneous rocks for four North American localities. *Economic Geology, 81,* 857-871.

[28] Rowan, L. C. & Mars, J. C. (2003). Lithologic mapping in the Mountain Pass, California, area using Advanced Space-borne Thermal Emission and Reflection Radiometer (ASTER) data. *Remote Sensing of Environment, 84,* 350-366.

[29] Rockwell, B. W., Clark, R. N., Livo, K. E., Mc Dougal, R. R., Kokaly, R. F. & Vance, J. S. (1999). Preliminary materials mapping in the Park City region for the Utah USGS-EPA Imaging Spectroscopy Project using both high and low altitude AVIRIS data. *In Summaries of the 8th Annual JPL Airborne Earth Science Workshop, R.O. Green, NASA-JPL, Pasadena, USA,* 365-375.

[30] Moghtaderi, A., Moore, F. & Mohammadzadeh, A. (2007). The application of advanced space borne Thermal

Emission and Reflection Radiometer (ASTER) data in Alteration mapping of Chadormalu paleocrater, Bafq region, central Iran. *Journal of Asian Earth Sciences, 30,* 238-252.

[31] Karnieli, A. (1997). Development and implementation of spectral crust index over dune sands. *International Journal of Remote Sensing, 18,* 1207-1220.

[32] Carranza, E. J. M. & Hale, M. (2002). Mineral imaging with Landsat Thematic Mapper data for hydrothermal alteration mapping in heavily vegetated terrane. *International Journal of Remote Sensing, 23,* 4827-4852.

[33] O'Neill, A. L. (1994). Reflectance spectra of microphytic soil crusts in semi-arid Australia. *International Journal of Remote Sensing, 15,* 675-681.

[34] Moghtaderi, A., Moore, F. & Mohammadzadeh, A. (2009). The application of advanced space borne Thermal Emission and Reflection Radiometer (ASTER) data in Alteration mapping of Chadormalu paleocrater, Bafq region, central Iran. *In 33rd International Geological Congress Oslo, Norway (2008), J. P. Derion (Ed.), published in Photo-Interpretation European Journal of Applied Remote Sensing* N 2009/2, 45, 79-87*, (2e trimestre 2009 ÉDITIONS ESKA, 12, rue du Quatre-Septembre, 75002 PARIS).*

[35] Svab, E., Tyler, A. N., Preston, T., Presing, M. & Baloch, K. V. (2005). Characterizing the spectral reflectance of algae in lake waters with high suspended sediment concentrations. *International Journal of Remote Sensing, 26,* 919-928.

[36] Lange, O. L., Kidron, G. J., Budel, B., Meyer, A., Kilian, E. & Abeliovich, A. (1992). Taxonomic composition and photosynthetic characteristics of the `biologic soil crust' covering sand dunes in western Negev Desert. *Functional Ecology, 6,* 519-527.

[37] Pichel, F. G., Cortez, A. L. & Nubel, U. (2001). Phylogenetic and morphological diversity of cyanobacteria in soil desert crusts from the Colorado plateau. *Applied and Environmental Microbiology, 67,* 1902-1910.

[38] Green, A. A. & Huntington, J. F. (1989). Remote sensing for surface mineralogy. *In Proceedings of Exploration'87: 3rd Decennial International Conference on Geophysical and Geochemical Exploration for Minerals and Groundwater, G. D. Garland, (Ed.),* 213-228.

[39] Kruse, F. A., Raines, G. L. & Watson, K. (1985). Analytical techniques for exerting geologic information from multichannel airborne spectroradiometer and airborne imaging spectrometer data. *Proceedings of the Fourth Thematic Conference on Geological Remote Sensing for Exploration Geology, Environmental Research Institute of Michigan (ERIM). Ann Arbor, Michigan.* 309-324.

[40] Kruse, F. A. (1988). Use of airborne imaging spectrometer data to map minerals associated with hydrothermally altered rocks in the northern Grapevine Mountains, Nevada, and California. *Remote Sensing of Environment, 24,* 31-51.

[41] Van der Meer, F. (1994). Calibration of Airborne Visible/Infrared Imaging Spectrometer Data (AVIRIS) to Reflectance and Mineral Mapping in Hydrothermal Alteration Zones: An example from "Cuprite Mining District". *Geocarto International, 3,* 23-37.

[42] Green, A. A., Bermann, M., Switzer, P. & Craig, M. D. (1988). A transformation for ordering multi-spectral data in terms of image quality with implications for noise removal. *IEEE Transactions on Geosciences and Remote Sensing, 26,* 65-74.

[43] Bordman, J. W. & Kruse, F. A. (1994). Automated spectral analysis: geologic example using AVIRIS data, north Grapevine Mountains, Nevada. *In Proceedings of the Tenth Thematic Conference on Geologic Remote Sensing, J. W. Boardman (Ed.), 407-408 (I. Ann Arbor: Environmental Research Institute of Michigan).*

[44] Castenholz, R. W. (1988). Culturing methods for cyanobacteria. *Methods in Enzymology, 167,* 68-93.

[45] Hughes, E. D., Gorham, R. & Zehnder. A. (1958). Toxicity of a unialgal culture of Microcystis aeruginosa. *Canadian Journal of Microbiology, 4,* 225-236.

[46] Allen, M. M. (1968). Simple conditions for growth of unicellular blue-green algae on plates. *Journal of Phycology, 4*, 1-3.

[47] Rippka, R. (1988). Isolation and Purification of cyanobacteria. *Methods in Enzymology, 167,* 3-27.

[48] Shirai, M., Matumaru, K., Ohotake, A., Takamura, Y., Aida, T. & Nakano, M. (1989). Development of a solid medium for growth and isolation of axenic Microcystis strains (Cyanobacteria). *Applied and Environmental Microbiology, 55,* 2569-2571.

[49] Belnap, J. (1995). Surface disturbances: their role in accelerating desertification. *Environmental Monitoring and Assessment, 37,* 39-57.

[50] Gons, H. J., Hakvoort, H., Peters, S. W. M. & Simis, S. G. H. (2005). Optical detection of cyanobacterial Blooms, shipboard observation and remote sensing. *In Huisman, J., Matthijs, H. C. P., Visser, P. M. (Ed.), Harmful Cyanobacteria, Netherland, Springer,* 177-199.

[51] Kutser, T., Metsama, L., Vahtmae, E. & Strombeck, N. (2006). Suitability of MODIS 250 m resolution band data for quantitative mapping of cyanobacterial blooms. *In: Proceeding of the Estonian Acad. Sci. Biol. Ecol, 55*(4), 318-328.

[52] Kutser, T. (2004). Quantitative detection of chlorophyll in cyanobacterial blooms by satellite remote sensing. *Limnology and Oceanography, 49,* 2179-2189.

[53] Metsama, L. & Kutser, T. (2008). On Suitability of MODIS Satellite Chlorophyll Products for the Baltic Sea Conditions. *Environmental Research, Engineering and Management, 44,* 4-9.

[54] Randolph, K., Wilson, J., Tedesco, L., Li, L., Pascual, D. L. & Soyeux, E. (2008). Hyperspectral remote sensing of cyanobacteria in turbid productive water using optically active pigments, chlorophyll a and phycocyanin. *Remote Sensing of Environment, 112,* 4009-4019.

[55] Simis, S. G. H., Peters, S. W. M. & Gons, H. J. (2005). Remote sensing of the cyanobacterial pigment phycocyanin in turbid inland water. *Limnology and Oceanography, 50,* 237-245.

IJST (2011) A1: 13-287
Iranian Journal of Science & Technology
http://www.shirazu.ac.ir/en

کاربرد داده های تصویری آستر (ASTER) و روش تخمین ریاضی (MEM) در ثبت و تشخیص سیانوباکتریهای موجود در پوسته زیست شناختی خاک، چادر ملو، ایران مرکزی

ا. مقتدری[1]، ف. مر[2]، س. م. تقوی[3] و ر. رضایی[3]

[1]گروه زمین شناسی، دانشکده علوم پایه، دانشگاه پیام نور، اوز، استان فارس، ایران
[2]بخش علوم زمین، دانشکده علوم، دانشگاه شیراز، شیراز، ایران
[3]بخش گیاه پزشکی، دانشکده کشاورزی، دانشگاه شیراز، شیراز، ایران

E-mail: a_moghtaderi@pnu.ac.ir or moghtaderiarsia@gmail.com

چکیده:

سطح خاکها در سرزمینهای خشک و نیمه خشک عاری از حیات گیاهی عالی است، اما بوسیله اجتماعی از موجودات زنده (نظیر سیانوباکتریها یا جلبکهای سبزآبی) پوشیده می شوند که قادر به تحمل شرایط سخت آب و هوایی بوده و بنابراین سازگار با شرایط بسیار خشک می باشند. در این پژوهش بشکلی شفاف و آشکار توانایی داده های سنجنده آستر (باندهای **VNIR**) در تشخیص پوسته زیست شناختی خاک یا پوسته های حاوی جلبکهای سبز آبی نشان داده می‌شود. روش پیشنهادی در این پژوهش (**MEM**) جدای از تقریبی بودن آن روشی سودمند در ثبت میکروارگانیسمها در مناطق غیر قابل دسترس از قبیل سطح دیگر سیارات یا مناطق دور از دسترس زمین می باشد.

Keywords: ASTER; cyanobacteria; MEM; remote sensing; biological soil crust